Computers and Concrete, *Vol. 16, No. 6 (2015) 825-846*
DOI: http://dx.doi.org/10.12989/cac.2015.16.6.825

Shear performance assessment of steel fiber reinforced-prestressed concrete members

Jin-Ha Hwang[1a], Deuck Hang Lee[2b], Min Kook Park[1c], Seung-Ho Choi[1d], Kang Su Kim[*] and Zuanfeng Pan[3e]

[1]Department of rchitectural Engineering, University of Seoul, 163 Seoulsiripdae-ro, Dongdaemun-gu, Seoul 130-743, Republic of Korea
[2]Department of Civil and Environmental Engineering, University of Illinois at Urbana-Champaign, 205 N. Mathews Ave. Urbana, IL 61801, USA
[3]Department of Building Engineering, Tongji University, 1239 Siping Road, Shanghai 200092, P.R. China

(Received July 1, 2015, Revised November 11, 2015, Accepted November 16, 2015)

Abstract. In this study, shear tests on steel fiber reinforced-prestressed concrete (SFR-PSC) members were conducted with test parameters of the concrete compressive strength, the volume fraction of steel fibers, and the level of effective prestress. The SFR-PSC members showed higher shear strengths and stiffness after diagonal cracking compared to the conventional prestressed concrete (PSC) members without steel fibers. In addition, their shear deformational behavior was measured using the image-based non-contact displacement measurement system, which was then compared to the results of nonlinear finite element analyses (NLFEA). In the NLFEA proposed in this study, a bi-axial tensile behavior model, which can reflect the tensile behavior of the steel fiber-reinforced concrete (SFRC) in a simple manner, was introduced into the smeared crack truss model. The NLFEA model proposed in this study provided a good estimation of shear behavior of the SFRPSC members, such as the stiffness, strengths, and failure modes, reflecting the effect of the key influential factors.

Keywords: SFRC; steel fiber; PSC, prestress; shear, nonlinear; FEM; shear strain

1. Introduction

It is generally recognized that prestressed concrete (PSC) members have advantages in deflection control as well as flexural strength, and, in particular, they have excellent shear performance compared to that of conventional reinforced concrete (RC) members. (Au *et al*. 2011,

*Corresponding author, Professor, E-mail: kangkim@uos.ac.kr
[a]Ph.D. Candidate, E-mail: jinhahwang@uos.ac.kr
[b]Research Scholar, E-mail: dlemrgod@illinois.edu
[c]Ph.D. Candidate, E-mail: mkpark@uos.ac.kr
[d]Ph.D. Candidate, E-mail: ssarmilmil@uos.ac.kr
[e]Assistant Professor, E-mail: zfpan@tongji.edu.cn

http://www.techno-press.org/?journal=cac&subpage=8 ISSN: 1598-8198 (Print), 1598-818X (Online)

Avendaño and Bayrak 2011, Lee and Kim 2011, Kim and Lee 2012a, b, Rahai and Shokoohfar 2012, Colajanni *et al*. 2014, Classen and Dressen 2015) Shear failure modes of PSC members, however, may be more brittle than conventional RC members. In order to improve the ductility and shear strength of PSC members as well as RC members, many recent studies suggested addition of steel fibers as an alternative (Narayanan and Darwish 1987, Tan *et al*. 1996, Padmarajaiah and Ramaswamy 2001, 2004, Furlan Jr. and Hanai 1999, Thomas and Ramaswamy 2006, Campione 2014, Colajanni *et al*. 2012, Dinh *et al*. 2010, Lee *et al*. 2011a, 2011b, 2013). Tan *et al*. (1996) conducted shear tests on T-beams made of steel fiber reinforced-prestressed concrete (SFR-PSC) with various levels of prestress (f_{pc}) and the volume ratio of steel fibers (V_f), and their test results were assessed by the shear behavior model based on the modified compression field theory (MCFT; Vecchio and Collins 1986). Padmarajaiah and Ramaswamy (2001, 2004) also conducted experimental tests on the SFR-PSC members cast with high strength concrete, based on which they proposed a simple equation for evaluation of shear strength of the SFRPSC members. Furlan Jr. and Hanai (1999) performed experimental study on the shear behavior of SFRPSC member with major variables of the volume ratio of steel fibers (V_f) and the shear reinforcement ratio (ρ_v), and they identified the amount of shear reinforcements required in shear design can be reduced significantly by considering the shear contribution of steel fibers at the crack interface. Despite the previous studies, however, the shear test data of SFR-PSC members are still insufficient to clearly understand their shear behavior, and particularly the ranges of test variables in previous studies are still very limited. Therefore, a total of 5 SFR-PSC beam specimens including a conventional PSC members without steel fibers were fabricated and tested in this study to investigate their shear strength, behavior, and failure mode. The test variables were the compressive strength of concrete (f_c'), the volume ratio of steel fibers (V_f), and the level of prestress (f_{pc}). The local and global behaviors of the SFRPSC members were analyzed by employing an image-based noncontact deformation measuring system, and their shear behavior was compared to the results of the nonlinear finite element analysis.

2. Numerical modeling approach

The tensile constitutive model of steel fiber-reinforced concrete (SFRC) material is an essential part in the analysis of shear behavior of SFR-PSC members. According to previous studies (Tan *et al*. 1996, Lee *et al*. 2012, 2013, Kim *et al*. 2012, Ju *et al*. 2012, Voo and Foster 2003, Minelli and Plizzari 2010), there are two types of approaches to consider the contribution of steel fibers on the shear behavior of SFR-PSC members. The first type is microscopic modeling approaches, in which the steel fibers at crack interface is modelled as independent steel reinforcements, and the bond behavior of steel fibers with surrounding concrete can be considered in the analysis of shear behavior. The second type is composite material modeling approaches, in which the SFRC material is treated as a fully composite material, and its tensile behavior is expressed by a constitutive curve. In this study, the second type approach was employed for an easy application to the nonlinear finite element analysis.

2.1 Derivation of biaxial constitutive model of SFRC in tension

In the SFRC members after diagonal cracking, the tensile resistance of steel fibers developed along the shear cracks is a major shear resistance mechanism, (Lee *et al*. 2012, Kim *et al*. 2012) by which the shear performance of the SFRC members is improved, compared to conventional RC members. In this study, the tensile behavior model of SFRC was derived, based on the SFRC panel test results reported by Susetyo (2009).

In Table 1, the details of the SFRC shear panel test specimens (Susetyo 2009) are summarized. The test specimens were 890×890×70 (mm) in size, in which the 8 mm diameter reinforcing bars (D8) were provided only in the horizontal direction. The compressive strengths of concrete used in the test specimens were 50 MPa and 80 MPa, and the test variables were the aspect ratio (L_f / D_f) and the volume fraction (V_f) of steel fibers. Fig. 1 illustrates the principal stress-strain behavior measured from the SFRC shear panel tests, in which the tensile stress-strain relationships of RC panels proposed by Vecchio and Collins (1986) and Hsu and Zhang (1996) are also shown together to examine the beneficial effects of steel fibers. The SFRC specimens showed improved post-cracking tensile resistance performance compared to conventional concrete. In particular, when the volume fractions of steel fibers (V_f) were larger than 1.0 %, their cracking strengths (f_{cr}) were maintained without softening after shear cracking or even slightly-hardening behaviors were observed. In this study, the tensile constitutive model of SFRC material subjected to biaxial stress was derived, modified from the Vecchio and Collins model, as follows

$$\sigma_1^f = E_{cf}\varepsilon_1 \le f_{cr,sfrc} \qquad \text{for} \quad \varepsilon_1 \le \varepsilon_{cr} \tag{1a}$$

$$\sigma_1^f = \frac{0.33\sqrt{f_c'} + 3F}{1 + (500\varepsilon_1)^{0.5(1-F)}} \qquad \text{for} \quad \varepsilon_1 > \varepsilon_{cr} \tag{1b}$$

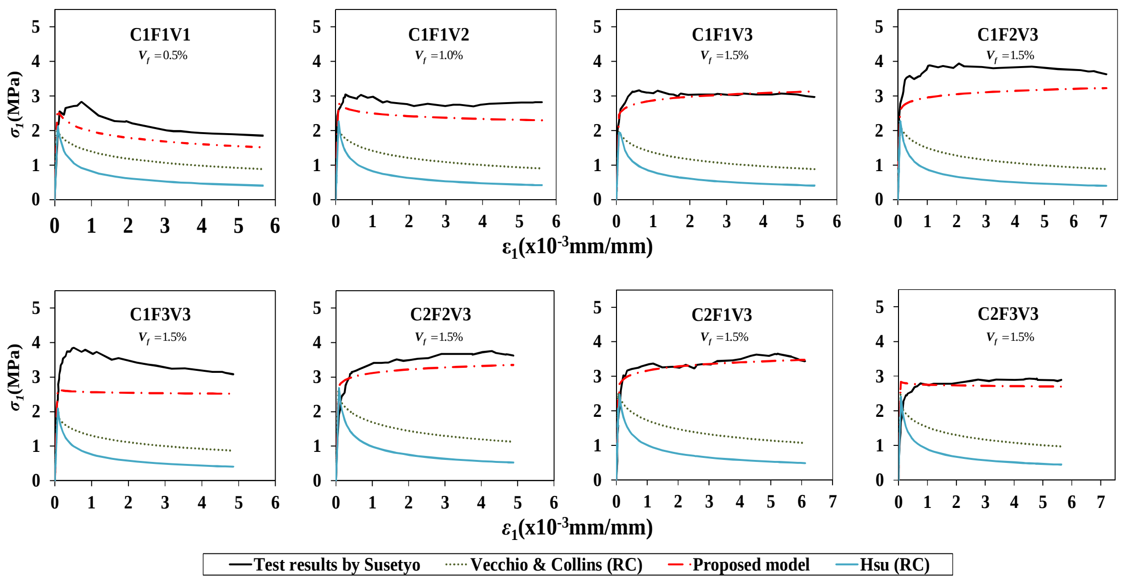

Fig. 1 Tensile behavior models for SFRC

Table 1 Details of SFRC shear panels (Susetyo 2009)

Name	V_f (%)	L_f (mm)	D_f (mm)	L_f/D_f	f'_c (MPa)	E_s (GPa)	f_y (MPa)
C1F1V1	0.5	50	0.62	81	51.4	224.7	552.2
C1F1V2	1.0	50	0.62	81	53.4	224.7	552.2
C1F1V3	1.5	50	0.62	81	49.7	224.7	552.2
C1F2V3	1.5	30	0.38	79	59.7	224.7	552.2
C1F3V3	1.5	35	0.55	64	45.5	224.7	552.2
C2F1V3	1.5	50	0.62	81	78.8	224.7	552.2
C2F2V3	1.5	30	0.38	79	76.5	224.7	552.2
C2F3V3	1.5	35	0.55	64	62	224.7	552.2

where the variable σ^f_1 is the tensile stress of SFRC, and E_{cf} is the elastic modulus of SFRC that can be taken as $2f'_c/\varepsilon'_c$. Here, f_c' and ε_c' are the compressive strength of concrete and its corresponding strain, respectively. Also, ε_1 is the tensile strain of SFRC, and $f_{cr,sfrc}$ the cracking strength of SFRC. By equating Eq. 1(a) and Eq. 1(b), the cracking tensile strain (ε_{cr}) can be obtained, and then $f_{cr,sfrc}$ can be easily calculated by inputting ε_{cr} into either of Eq. 1(a) and Eq. 1(b). The fiber coefficient is $\eta V_f d_f$, and η is the aspect ratio (=L_f / D_f) of steel fibers, L_f and D_f are the length and the diameter of steel fibers, respectively, V_f and d_f and are the volume fraction and the bond coefficient of steel fibers, respectively. The bond coefficient (d_f) were adopted to be 1.0 for hooked fibers, 0.75 for crimped fibers, and 0.5 for straight fibers. As aforementioned, Eq. 1(b) was modified from the tension stiffening curve for RC members without fibers, which was developed by Vecchio and Collins. In the development of Eq. 1(b), the fiber factor (F) was summated on the numerator to reflect the increase of cracking strength by addition of steel fibers, and was put on the exponent part of the tensile strain term to reflect the increase of residual tensile stress of SFRC due to steel fibers. The coefficients of the fiber factors in the denominator and the numerator were then determined by fitting to test results. As shown in Fig. 1, Eq. (1) estimates the cracking strengths and the post-cracking tensile behaviors of SFRC shear panels very closely.

In this study, the constitutive model of SFRC in tension expressed in Eq. (1) was utilized in the nonlinear finite element analysis (NLFEA) program Vector 2 (Vecchio and Wong 2002) by using the strain-based custom tension stiffening model. As illustrated in Fig. 2, the tensile behavior curve calculated through Eq. (1) was idealized by total 4 major points in the Vector 2 program platform, and the maximum tensile strain capacity of SFRC material was defined as follows

$$\varepsilon_{tu} = \omega_u / l^* \tag{2}$$

where ω_u is the maximum crack opening displacement (COD). (Lim *et al*. 1987) The value of ω_u was used as L_f / 16 when the prestress (f_{pc}) was less than or equal to 5MPa, as proposed by Lim *et al*. (1987) When the prestress (f_{pc}) was over 5MPa, it was reduced to L_f /8 to consider the enhancement of crack control ability due to the synergistic effects of steel fibers and the prestress in an approximation manner. Also, l^* is the reference length, which was calculated by using the average shear crack spacing ($s_{m\theta}$) of SFRC, as follows

$$s_{m\theta} = \frac{s_{mx}}{\sin\theta} \tag{3}$$

where s_{mx} is the crack spacing in the longitudinal direction of the member, and crack spacing estimation model proposed by Dupont and Vandewalle (2003) was adopted to take account of the improved crack control capacity provided by steel fibers, as follows:

$$s_{mx} = \left(50 + 0.25 k_1 k_2 \frac{d_b}{\rho_{x,eff}}\right) \cdot \left(\frac{50}{L_f / D_f}\right) \tag{4}$$

where k_1 is the bond coefficient of steel fibers, and 0.8 and 0.4 were taken for round and deformed reinforcing bar, respectively, k_2 is the strain gradient factor, which is used as 1.0 in this study for simplification. (Collins and Mitchell 1991) Also, d_b and $\rho_{x,eff}$ are the diameter and the effective ratio of longitudinal reinforcement, respectively (CEB-FIP 1978, ENV 1992-1-1 1991).

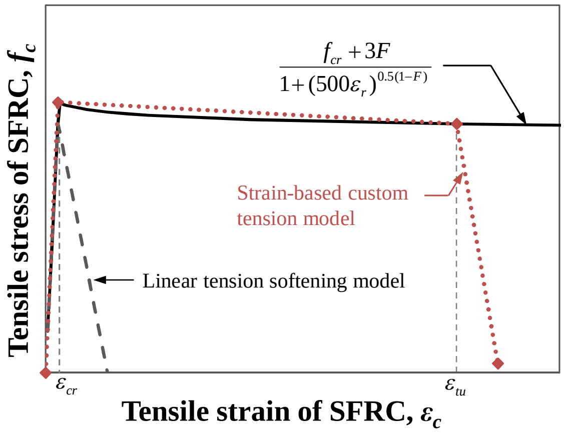

Fig. 2 Strain-based tension stiffening modeling approach

Table 2 Material properties of concrete

Specimen name	f_c' (MPa)	ε'_c
HP0F1	67.8	0.0027
NP1F0	43.8	0.002
HP1F1	65.4	0.0028
NP2F1	42.6	0.0024
HP2F1	57.1	0.0024

3. Experimental program

3.1 Material properties

The compressive strength of concrete (f_c') and its corresponding strain (ε'_c) of test specimens are summarized in Table 2. The characters of H and N in the specimen names denote the high strength concrete and the normal strength concrete, respectively. The material test results of

Table 3 Material properties of reinforcing bars and tendons

Bar type	f_y (MPa)	ε_y	E_s (GPa)	f_u (MPa)
D22	460	0.00253	181	584
D13	383	0.00254	151	553
7 wire - ϕ12.7	1770	0.01100	200	1936

Table 4 Material properties of steel fibers

Shape	L_f (mm)	D_f (mm)	f_u (MPa)
Hooked type	30	0.5	981

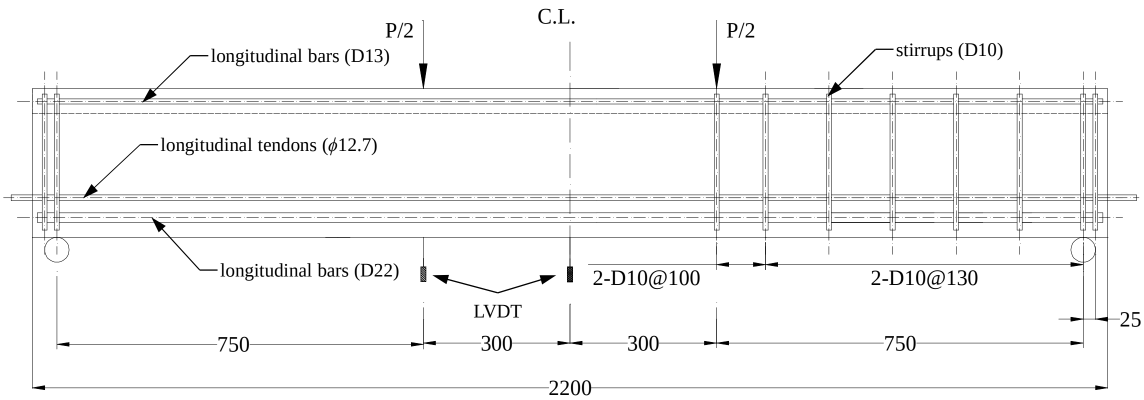

(a) Details of specimens and measurement devices

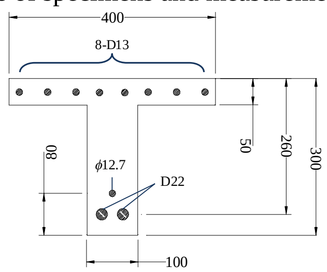

(b) Sectional details

Fig. 3 Details of specimens and test set-up

reinforcing bars and tendons are summarized in Table 3. The hooked steel fibers with an aspect ratio (η) of 60.0 were used in all the test specimen and their material properties are shown in Table 4.

3.2 Specimen details and loading

The details of test specimens and their test set-up are illustrated in Fig. 3. The span length of test specimens was 2,100 mm, and the length of shear span (a) was 750 mm. As shown in Fig. 3(a), the transverse reinforcement was not provided on the left shear span of all the test specimens, while sufficient stirrups with a spacing of 130mm were provided on the rifht shear span to prevent the shear failure.

Table 5 shows test variables of the specimens; the magnitude of introduced prestress (f_{pc}), the volume fraction of steel fibers (V_f), the tensile reinforcement ratio (ρ_s), and the tendon ratio (ρ_p). While HP0F1 specimen was non-prestressed, NP1F0 and HP1F1 specimens (P1 series) were prestressed, and their average prestress (f_{pc}) was 2.95 MPa. The average prestress (f_{pc}) of NP2F1 and HP2F1 specimens (P2 series) were 5.24 MPa. Two D22 reinforcing bars were commonly provided for all the test specimens, and a ϕ12.7 tendon was placed on the test specimens prestressed by 2.95MPa, while two ϕ12.7 tendons were provided on the test specimens prestressed by 5.24MPa. For the non-prestressed specimen HP0F1, a D13 reinforcing bar was additionally provided to secure the same flexural strength as the prestressed specimens. The volume fraction of steel fibers was 1.5% for all the test specimens except NP1F0 specimen that had no steel fiber. All the test specimens were loaded at 2-points by the deformation control as illustrated in Fig. 3(a), and the LVDTs were placed at the center and loading points of the each specimen to measure their deflection.

Table 5 Details of test specimens

Specimen name	f_{pc} (MPa)	V_f (%)	ρ_s (%)	ρ_p (%)
HP0F1	0	1.5	3.46	0
NP1F0	2.95	0	2.98	0.38
HP1F1	2.95	1.5	2.98	0.38
NP2F1	5.24	1.5	2.98	0.76
HP2F1	5.24	1.5	2.98	0.76

Table 6 Cracking and ultimate strengths of specimens

Specimen name	P_{cr} (kN)	P_{dcr} (kN)	P_u (kN)	$P_{n,ACI}$ (kN)	$P_{n,MC2010}$ (kN)
HP0F1	151.9	162.0	295.0	124.1	209.4
NP1F0	(116.0)*	125.0	132.7	146.2	116.0
HP1F1	124.4	199.0	320.3	168.4	228.2
NP2F1	181.3	247.9	336.1	192.3	223.3
HP2F1	171.5	223.4	424.1	176.7	242.2

* Flexural cracks appeared after 2nd drop of loading caused by diagonal cracks, i.e., at 7.1 mm in deflection (See Fig. 4)

P_{cr}: flexural cracking load, P_{dcr}: diagonal cracking load, P_u: ultimate load

4. Test results

4.1 Load-deflection behavior

The flexural cracking load (P_{cr}), the shear cracking load (P_{dcr}), and the ultimate load (P_u) of test specimens are summarized in Table 6, and the load-deflection behavior are shown in Fig. 4, in which the markers indicates the diagonal cracking loads. Also, the shear strengths, calculated by the equation for PSC members presented in ACI318-11 ($P_{n,ACI}$) and the equation for SFRPSC

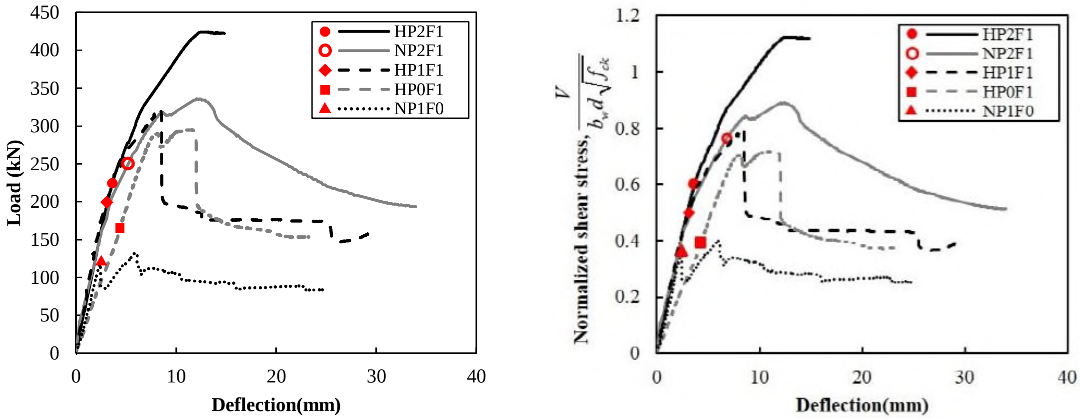

(a) Load-deflection responses (b) Normalized shear stress-deflection responses

Fig. 4 Measured behavior curves of specimens

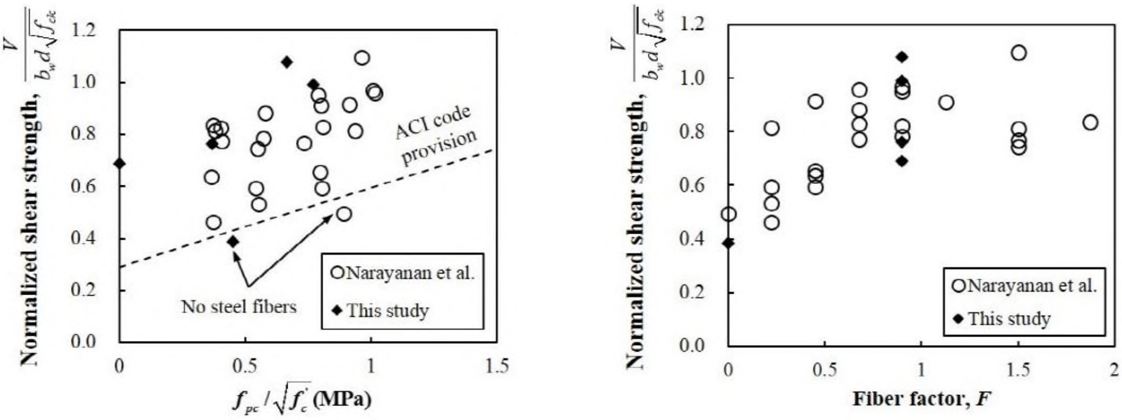

(a) Effect of prestress on shear strength (b) Effect of fiber factor on shear strength

Fig. 5 Effects of key influential factors on normalized shear strength

members represented in MC2010 ($P_{n,MC2010}$), are shown in Table 6. In applying MC2010, the tensile stress of concrete at the crack width (w) of 1.5 mm was evaluated using the Variable Engagement Model (VEM) proposed by Voo and Foster (2009).

Note that these equations, i.e., ACI318-11, MC2010 and VEM, are presented in APPENDIX A. The test specimens with the high level of prestress showed the higher flexural cracking strengths. The NP1F0 test specimen with no steel fiber, however, had the diagonal cracking on the web concrete before flexural cracking occurred. As shown in Fig. 4(a), the test specimens reinforced with steel fibers had higher diagonal cracking strengths (P_{dcr}) compared to the NP1F0 test specimens without steel fiber, and the NP2F1 and HP2F1 test specimens (P2 series) with high level of prestress showed higher diagonal cracking strengths. It was also shown that the NP1F0 test specimen without steel fiber and a low level of prestress showed the lowest shear strength, while the HP2F1 test specimen with steel fiber and a high level of prestress showed the highest strength and stiffness. It should be noted that, in the case of HP2F1 test specimen, the post- peak

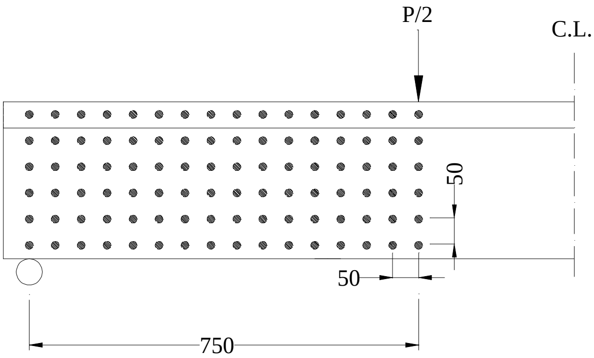

(a) Location of target points

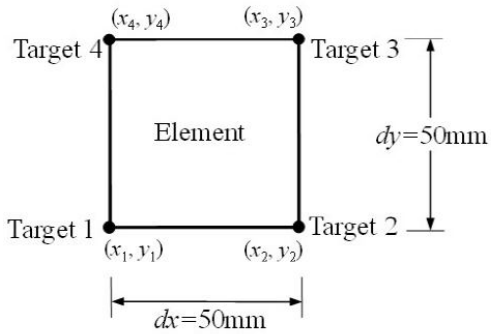

(b) Target coordination

(c) Installation of image-based measurement device

Fig. 6 Details of three dimensional image-based measurement system

deformation data could not be obtained due to the malfunction of measurement device after the peak. The HP1F1 specimen showed the higher strength and stiffness compared to the HP0F1 specimen due to the prestress, and the specimens HP2F1 and NP2F1 with a high level of prestress showed more improved shear strengths and ductile behavior compared to those of P0 and P1 series specimens. This can be confirmed more clearly in the normalized shear stress-deflection curves shown in Fig. 4(b).

The shear strengths of test specimens except NP1F0 showed higher than those estimated by ACI318-11(2011) due to the contribution of steel fibers. The test specimens also showed higher shear strength than those calculated by MC2010(2012), which means that the equation in MC2010 was proposed conservatively for safety purpose.

Fig. 5 represents the normalized shear strengths obtained from this study and Narayanan and Darwish (1987). The detailed information of SFR-PSC specimens tested by Narayanan and Darwish (1987) is attached on the Appendix B. Note that the test results of two PSC beam specimens without steel fiber was included as reference points. As illustrated in Fig. 5(a), there is an increasing tendency in their shear strengths proportional to the magnitude of $f_{pc}/\sqrt{f_c'}$. All the specimens reinforced with steel fibers showed higher shear strengths than the web-shear (cracking) strength specified in ACI318-11 (2011), while the two specimens without steel fiber showed lower shear strengths than that specified in ACI318-11 (2011). Fig. 5(b) also shows an increasing trend of their shear strengths proportional to the amount of steel fibers.

4.2 Shear strain distribution and nonlinear finite element analysis

In this study, an image-based non-contact displacement measurement device was employed to measure the 3-dimensional local and global shear behaviors of test specimens as shown in Fig. 6. The 3-dimensional displacement information was measured from movement of the targets attached on the surface of the test specimens by 50mm spacing. As shown in Fig. 6(b), the shear strain (γ_{xy}) was calculated by using the coordinates of adjacent four targets with 50mm spacing, as follows

$$\gamma_{xy} = \frac{\left(\left(x_4 - x_1\right)/dy + \left(x_3 - x_2\right)/dy\right) + \left(\left(y_2 - y_1\right)/dx + \left(y_3 - y_4\right)/dx\right)}{2} \tag{5}$$

Fig. 7 shows the shear strain distributions calculated by Eq. (5) based on the measured data right after the diagonal shear cracking (P_{dcr}). In Fig. 7(a), the NP1F0 specimen with no steel fiber showed very large shear deformations localized at the diagonal cracking region, and the shear strain elsewhere was very small. In the other test specimens with steel fibers, although the deformations were still concentrated on the region near diagonal shear cracks to some extent, the crack widths were well controlled within 10% ~ 24% level of the NP1F0 specimen.

Fig. 8 shows the distribution of shear strains at maximum load (P_u), from which it can be seen that the deformation of all the five test specimens was concentrated on near the cracking region. The specimens NP1F0 and HP0F1 showed the largest shear strain at the center of their shear span where the critical shear cracks were observed. The HP1F1 specimen showed a lower crack angle compared to that of the HP0F1 specimen due to the effect of prestress. The crack angles of the

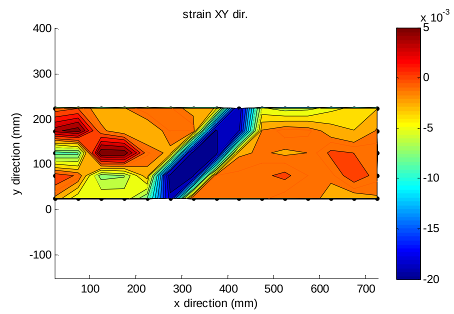

(a) NP1F0 specimen

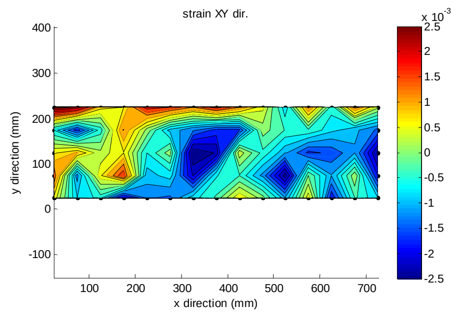

(b) HP0F1 specimen

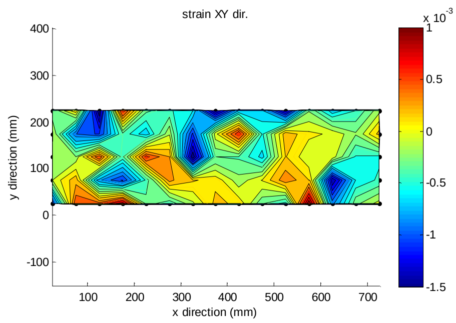

(c) HP1F1 specimen

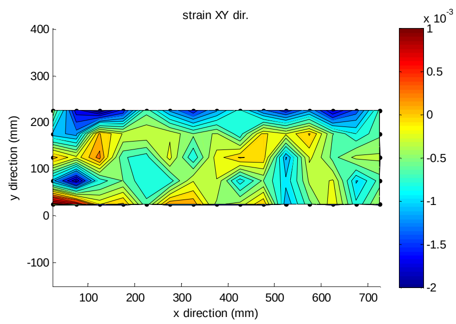

(d) NP2F1 specimen

Fig. 7 Shear strain distribution right after diagonal cracking

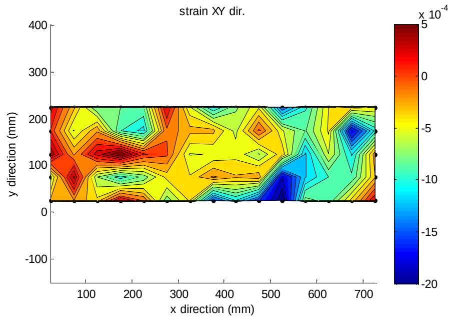

(e) HP2F1 specimen

Fig. 7 Continued

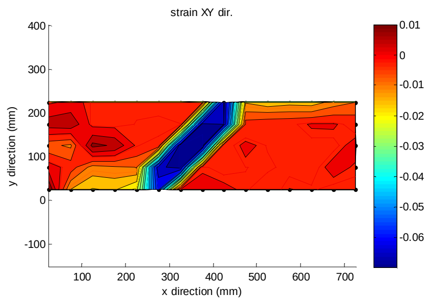

(a) NP1F0 specimen

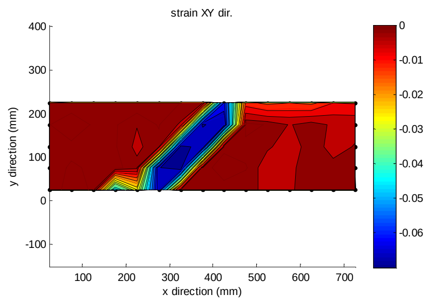

(b) HP0F1 specimen

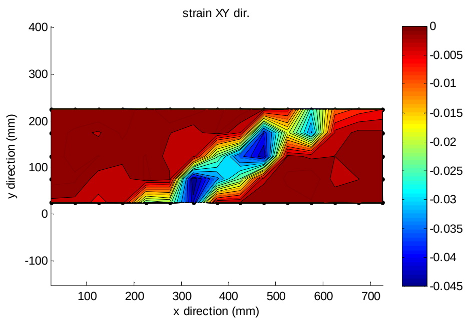

(c) HP1F1 specimen

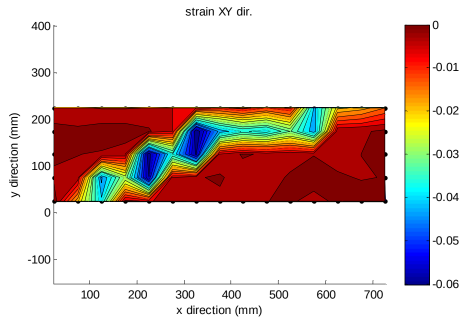

(d) NP2F1 specimen

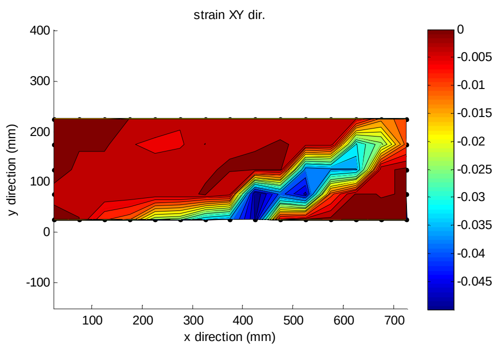

(e) HP2F1 specimen

Fig. 8 Shear strain distribution at ultimate specimens NP2F1 and HP2F1 were the lowest, and the diagonal tension failures were observed near the supporting point for the NP2F1 specimen and around the loading point for the HP2F1 specimen. Fig. 9 illustrates the crack patterns of the NP1F0 and HP1F1 specimens at different loading stages, and Figure 10 shows the crack patterns of all the test specimens at their ultimate state. From the comparison of Figs. 7(a) and 9(a), it can be confirmed that the diagonal cracking occurred at the location where the shear deformation was concentrated. Particularly, the NP1F0 specimen experienced the shear cracking before the occurrence of flexural cracking, and the crack width measured right after the shear cracking appeared very large (1.8 mm). The maximum shear crack width at the maximum load was about 5.9 mm as illustrated in Fig. 9(b), and a significant increase of the shear crack width was observed in its post-peak behavior until the deflection reached 15 mm as shown in Fig. 9(c), while the flexural crack widths remained almost constant. In addition, as shown in Fig. 9(c), the severe bond cracks finally developed along the tensile reinforcing bars provided in the bottom of the section. In case of the HP1F1 specimen shown in the right side of Fig. 9, the flexural cracks occurred in the shear span, and a flexural-shear crack was developed after the flexural cracks propagated into the centroidal axis of the cross section at the maximum moment region. The maximum shear crack width of the HP1F1 specimen measured right after the shear cracking and at the ultimate load were 0.1 mm and 1.9 mm, respectively, which implies that the crack width of the HP1F1 specimen was well-controlled compared to those of the NP1F0 specimen. However, it was found that the shear crack width increased rapidly similar to that of the NP1F0 test specimen after reaching its ultimate load, which is considered to be accompanied by the pull-out failure of steel fibers.

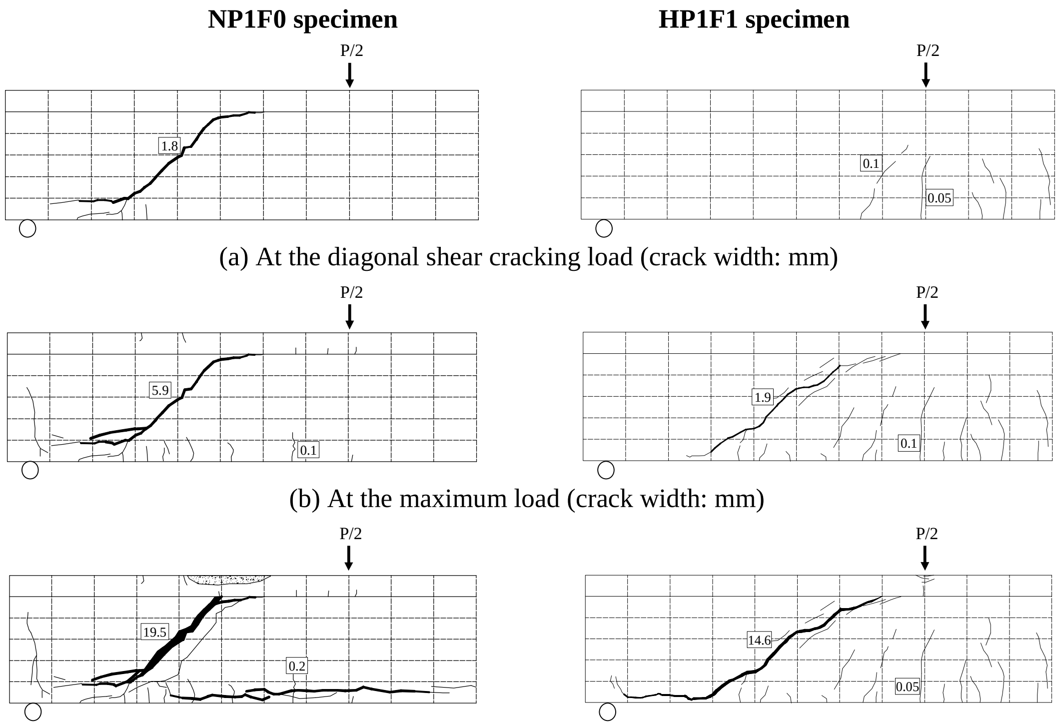

(a) At the diagonal shear cracking load (crack width: mm)

(b) At the maximum load (crack width: mm)

(c) At the deflection of 15mm (crack width: mm)

Fig. 9 Crack patterns of NP1F0 and HP1F1 specimens at different loading stages

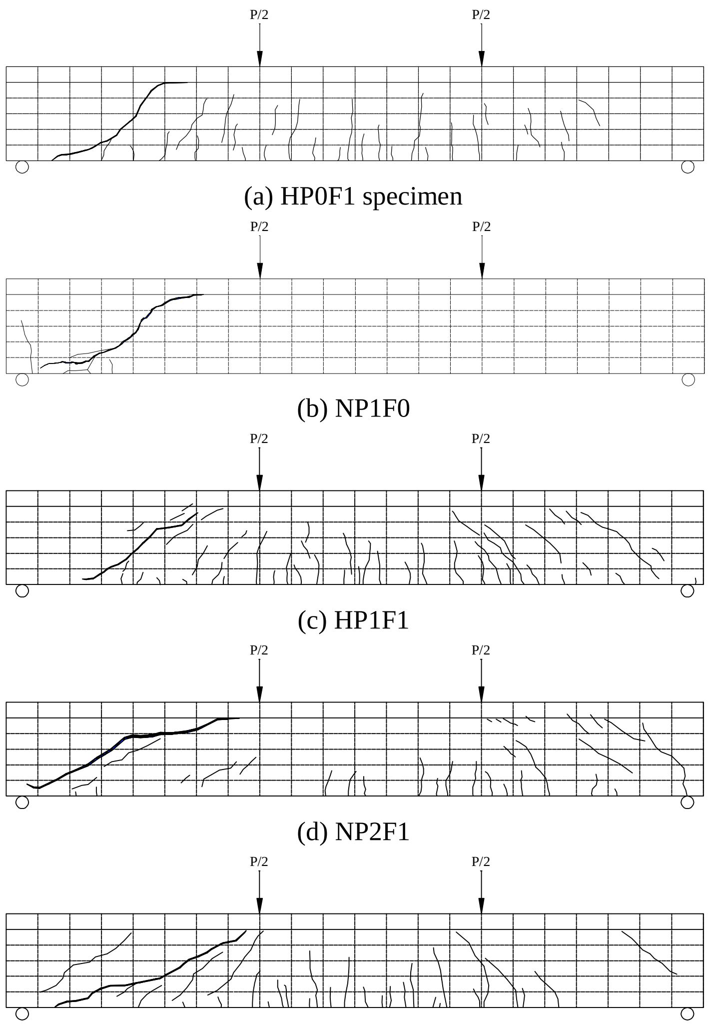

(a) HP0F1 specimen

(b) NP1F0

(c) HP1F1

(d) NP2F1

(e) HP2F1

Fig. 10 Crack patterns of test specimens at ultimate

This behavioral characteristics will be explained in the next section based on the analysis results. It can be also noted that the cracking patterns of all the specimens at the ultimate state shown in Fig. 10 are consistent with the shear strain distributions shown in Fig. 8.

5. Analysis and verification

The shear failure of slender concrete beam members typically occurs by losing the shear resistance of web concrete due to the shear crack propagation and opening after diagonal cracking. The shear failure modes of slender SFRC beam members are also often similar to this, but it can secure higher strength and ductility due to the tensile resistance of steel fibers after the shear cracking. The tensile stress of steel fibers gradually increases as the crack width increases after the diagonal cracking, and even when the stress of steel fibers reaches their bond strength, the shear ductility of the SFRC member can be secured by their residual bond stress up to a certain level of deformation. (Lee *et al*. 2012, Kim *et al*. 2012, Ju *et al*. 2012, Lim *et al*. 1987)

When the slip between steel fibers and concrete reaches a certain limit of deformation, the steel fibers are pulled out due to the loss of the bond resistance, and thereby the shear resistance of the SFRC member decreases rapidly. In Fig. 2, the point at which the stress decreases rapidly implies this phenomenon, which will be also discussed here based on the NLFEA results from now on.

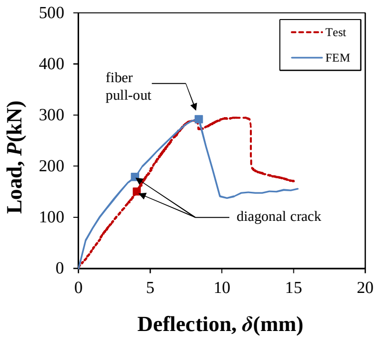

(a) HP0F1 specimen

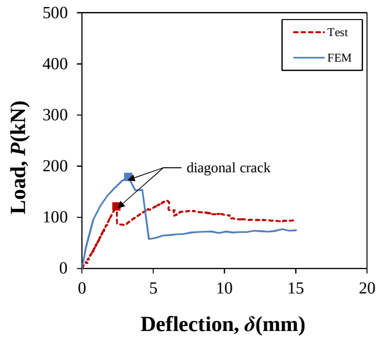

(b) NP1F0 specimen

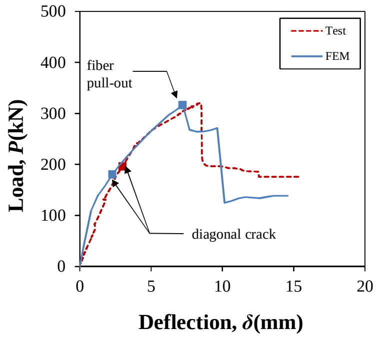

(c) HP1F1 specimen

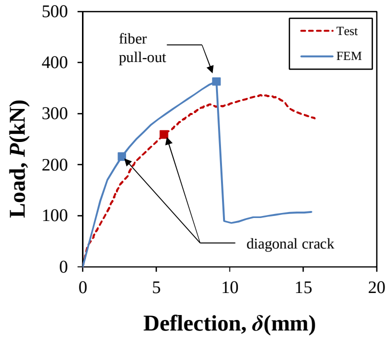

(d) NP2F1 specimen

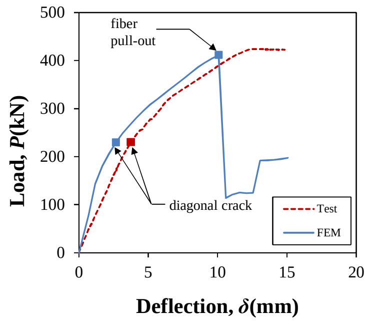

(e) HP2F1 specimen

Fig. 11 Verification of NLFEA

Table 7 Verification of nonlinear FE Analysis

Specimen name	$P_{u,test}$ (kN)	$P_{u,FEM}$ (kN)	$P_{u,test}$ / $P_{u,FEM}$
HP0F1	295.0	291.6	1.01
NP1F0	132.7	180.8	0.73
HP1F1	320.3	316.4	1.01
NP2F1	336.1	362.6	0.93
HP2F1	424.1	411.4	1.03
	Avg.		0.94
	SD		0.12
	COV		0.13

In Fig. 11, the results of NLFEA are compared to the test results, and the comparisons of the member strengths are presented in Table 7. In the finite element modeling, the SFRC were modeled as rectangular elements with a mesh dimension of 50×50 mm.

The compressive stress-strain relationships proposed by Hognestad (1951) and Nataraja *et al*. (2009) were used for pre-peak and post-peak behavior, respectively. It is noted that the SFRC material model was applied in only post-peak behavior, and that the RC material model was used for pre-peak behavior, which is because steel fibers does not influence the pre-peak behavior in compression as reported by many researchers. (Choi *et al*. 2007, ACI Commmitte 544 1988, Tan and Mansur 1990, Tan *et al*. 1992, Susetyo 2009, Spinella *et al*. 2012) The elasto-plastic model and the Ramberg-Osgood model (Mattock 1979) were used for re-bars and tendons, respectively.

As shown in Fig. 11(a), the analysis model predicted the point of diagonal cracking, ultimate strength of the HP0F1 specimen with a good accuracy. The pull-out point of steel fibers shown in Fig. 11(a) does correspond with the point where the tensile strain obtained from the NLFEA reaches the in Fig. 2. Thus, the analysis result of the HP0F1 specimen indicates that it failed by the pull-out of steel fibers after their principal tensile strains reached.

The analysis results of the NP1F0 specimen shown in Fig. 11(b) provided the diagonal cracking strength and ultimate strength significantly different from the test results, compared to other test specimens. The shear strength of NP1F1 specimen was much lower than the existing test results as shown in Fig. 5 and that estimated by current code provisions. In fact, it is widely known that the shear strengths of the reinforced concrete members without shear reinforcement including PSC members vary with a large range of scatter due to the sudden failure characteristics of diagonal cracking. (Jung and Kim 2008) It is, however, worthy of noting that the rapid decreasing behavior after the diagonal cracking in the NP1F0 specimen were simulated similarly in the NLFEA results. For the HP1F1 specimen represented in Fig. 11(c), the NLFEA provided very close simulation of the diagonal cracking strength, stiffness and ultimate strength of the test specimen, and in particular, the load increase after the diagonal cracking and the failure with rapid load reductions resulting from the pull-out of steel fibers after the peak load were simulated very accurately. As shown in Figs. 11(d) and (e), the NLFEA also provided very close simulation results on the load-deflection behavior of the specimens NP2F1 and HP2F1, except that the rapid decrease of load after the peak was not observed in the test results. This seems to be attributable to maintaining the resistance mechanism in tension side of the members enabled by the relatively high level of prestress.

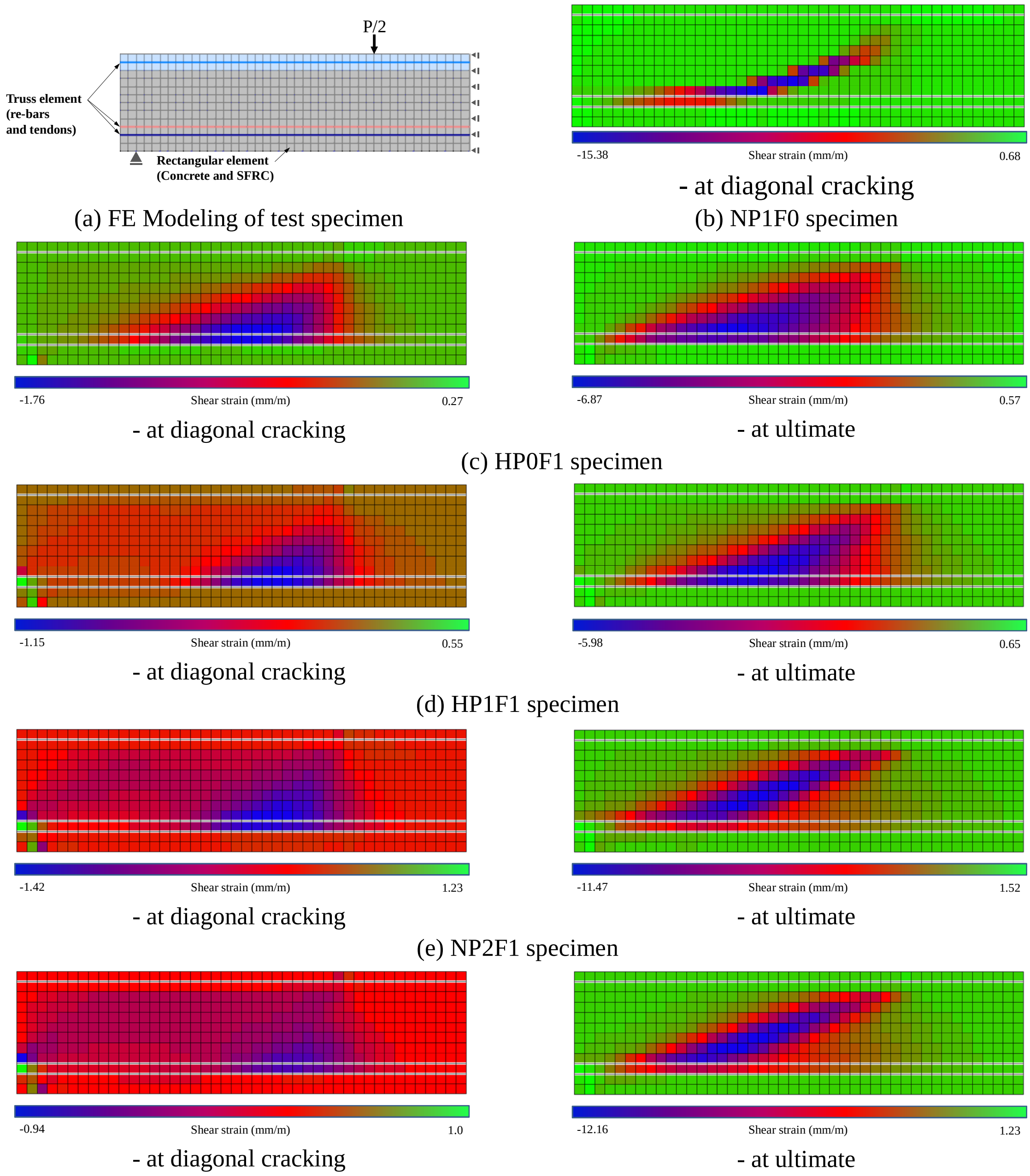

(a) FE Modeling of test specimen (b) NP1F0 specimen

(c) HP0F1 specimen

(d) HP1F1 specimen

(e) NP2F1 specimen

(f) HP2F1 specimen

Fig. 12 Shear strain distributions simulated by NLFEA

Fig. 12 shows the shear strains obtained from the NLFEA. The FE Modeling is shown briefly in Fig. 12(a), and the shear strains of the specimens at diagonal cracking are presented on the left side of Figs. 12(c) to (f) while the shear strains at ultimate are shown on the right side of the figures. The analysis results of the NP1F0 specimen shown in Fig. 12(b) indicate that the diagonal crack was formed from the loading point to the support connected by the horizontal crack along the tendon and reinforcing bars, which coincides with the observations from the test result shown in Fig. 9(a). The analysis results of the HP0F1 specimen showed large shear deformations at diagonal cracking and at ultimate along the compression fields, and the shear deformations were distributed more extensively over the wide range of the web, compared to the NP1F0 specimen. The distributions of shear deformation at diagonal cracking looks like very similar to those at ultimate; looking at them in detail, however, there is some difference. It can be found that the shear deformations were more concentrated on near the loading points at diagonal cracking, while they moved to near the support at ultimate. It is considered that, as the applied shear force gets greater, the direction of diagonal force becomes flatter and the longitudinal tension force near the support increases. Consequently, the shear deformations are more concentrated on near the support at ultimate, which is possible because the shear stresses can be sustained by the resistance of steel fibers after the initial shear cracking. Such a tendency can also be observed from other SFR-PSC members presented in Figs. 12(d) to (f).

6. Conclusions

In this study, shear tests on SFR-PSC members were conducted with test parameters of the concrete compressive strength, the volume fraction of steel fibers, and the level of effective prestress. The shear deformations of the specimens were measured by a non-contact 3D displacement measurement device, which were then compared to the results of NLFEA. Based on this study, the following conclusions were obtained.

• The SFR-PSC beam specimens had higher stiffness and strength than the PSC beam specimen without steel fibers, and their shear strengths increased as the concrete compressive strength or the level of prestress increased.

• The tensile behavior of SFRC were implemented in the nonlinear finite element analysis (NLFEA), and the shear strength and behavior of the SFR-PSC members were very closely simulated by the NLFEA.

• The non-contact 3D displacement measurement device was very useful for measuring the web shear strains of the specimens, and made it possible to observe the distribution of shear strains very clearly.

• The proposed NLFEA simulated the distribution of shear strains of the specimens at diagonal cracking and at the ultimate very similarly.

Acknowledgements

This work was supported under the framework of international cooperation program managed by National Research Foundation of Korea (No.2014K2A2A2000659)

References

ACI Committee 318 (2008), *Building code requirements for structural concrete (ACI 318M-08) and Commentary*, American Concrete Institute, Farmington Hills.

ACI Committee 544 (1988), *Design consideration for steel fiber reinforced concrete (ACI 544.4R-88)*, *ACI Struct. J.*, **85**(5), 563-580.
Adebar, P. and Collins, M.P. (1996), "Shear strength of members without transverse reinforcement", *Can. J. Civil Eng.*, **23**(1), 30-41.
Au, F.T.K., Leung, C.C.Y. and Kwan, A.K.H. (2011), "Flexural ductility and deformability of reinforced and prestressed concrete sections", *Comput. Concrete*, **8**(4), 473-489.
Avendaño, A.R. and Bayrak, O. (2011), "Efficient shear reinforcement design limits for prestressed concrete beams", *ACI Struct. J.*, **108**(6), 689-697.
CEB-FIP (1978), *Model code for concrete structures*, CEB-FIP International Recommendations, 3rd Edition, Comité Euro-International du Béton, Paris.
Fib draft Model Code (2012), *Model Code 2010***-** fib Bulletin No. 65. Final draft
Campione, G. (2014), "Flexural and shear resistance of steel fiber–reinforced lightweight concrete beams", *J. Struct. Eng.*, **140**(4).
Classen, M. and Dressen, T. (2015), "Experimental investigations on prestressed concrete beams with Openings", *ACI Struct. J.*, **112**(2), 221-232.
Choi, K.K., Park, H.G. and Wight, J.K. (2007), "Shear strength of steel fiber-reinforced concrete beams without web reinforcement", *ACI Struct. J.*, **104**(1), 12-21.
Colajanni, P., Recupero, A. and Spinella, N. (2014), "Design procedure for prestressed concrete beams", *Comput. Concrete*, **13**(2), 235-253.
Colajanni, P., Recupero, A. and Spinella, N. (2012), "Generalization of shear truss model to the case of SFRC beams with stirrups", *Comput. Concrete*, **9**(3), 227-244.
Collins, M.P. and Mitchell, D. (1991), *Prestressed concrete structures*, Prentice-Hall.
Dinh, H.H., Parra-Montesinos, G.J. and Wight, J.K. (2010), "Shear behavior of steel fiber-reinforced concrete beams without stirrup reinforcement", *ACI Struct. J.*, **107**(5), 597-606.
Dupont, D. and Vandewalle, L. (2003), "Calculation of crack widths with the s-e method", *Test and design methods for steel fibre reinforced concrete: background and experiences-Proceedings of the RILEM TC162-TDF Workshop*, RILEM Technical Committee 162-TDF, Bochum, Germany, 119-144.
ENV 1992-1-1 (1991), *Eurocode 2: design of concrete structures* **-** *Part 1.1: General rules and rules for buildings*.
Furlan Jr., S. and Hanai, J.B. (1999), "Prestressed fiber reinforced concrete beams with reduced ratios of shear reinforcement", *Cement Concrete Comp.*, **21**(3), 213-221.
Hognestad, E. (1951), *A study of combined bending and axial load in rein forced concrete members*, University of Illinois Engineering Experimental Station, Bulletin Series No. 399
Hsu, T.T.C. and Zhang, L. (1996), "Tension stiffening in reinforced concrete membrane elements", *ACI Struct. J.*, **93**(1), 108-115.
Ju, H., Lee, D.H., Hwang, J.H., Kang, J.W., Kim, K.S. and Oh, Y.H. (2012), "Torsional behavior model of steel-fiber-reinforced concrete members modifying fixed-angle softened-truss model", *Compos. Part B Eng.*, **45**(1), 215-231.
Jung, S. and Kim, K.S. (2008), "Knowledge-based prediction of shear strength of concrete beams without shear reinforcement", *Eng. Struct.*, **30**(6), 1515-1525.
Kim, K.S. and Lee, D.H. (2012), "Flexural behavior model for post-tensioned concrete members with unbonded tendons", *Comput. Concrete,* **10**(3), 241-258.
Kim, K.S., Lee, D.H., Hwang, J.H. and Kuchma, D.A. (2012), "Shear behavior model for steel fiber-reinforced concrete members without transverse reinforcements", *Compos. Part B: Eng.*, **43**(5), 2324-2334.
Kim, K.S. and Lee, D.H. (2012), "Nonlinear analysis method for continuous posttensioned concrete members with unbonded tendons", *Eng. Struct.*, **40**(1), 487-500.
Lee, D.H. and Kim, K.S. (2011), "Flexural strength of prestressed concrete members with unbonded tendons", *Struct. Eng. Mech.*, **38**(5), 675-696.
Lee, D.H., Hwang, J.H., Ju, H.J. and Kim, K.S. (2014), "Application of direct tension force transfer model with modified fixed-angle softened-truss model to finite element analysis of steel fiber-reinforced

concrete members subjected to shear", *Comput. Concrete*, **13**(1), 49-70.
Lee, D.H., Hwang, J.H., Ju, H., Kim, K.S. and Kuchma, D.A. (2012), "Nonlinear finite element analysis of steel fiber-reinforced concrete members using direct tension force transfer model", *Finite Elem. Anal. Des.*, **50**(1), 266-286.
Lee, S.C., Cho, J.Y. and Vecchio, F.J. (2011a), "Diverse embedment model for steel fiber-reinforced concrete in tension: model development", *ACI Mater. J.*, ***108***(5), 516-525.
Lee, S.C., Cho, J.Y. and Vecchio, F.J. (2011b), "Diverse embedment model for steel fiber-reinforced concrete in tension: model verification", *ACI Mater. J.* ***108***(5), 526-535.
Lee, S.C., Cho, J.Y. and Vecchio, F.J. (2013), "Tension-stiffening model for steel fiber-reinforced concrete containing conventional reinforcement", *ACI Struct. J.*, ***110***(4), 639-648.
Lim, T.Y., Paramsivam, P. and Lee, S.L. (1987), "Analytical model for tensile behavior of steel-fiber concrete", *ACI Mater. J.*, **84**(4), 286-298.
Mattock, A.H. (1979), "Flexural strength of prestressed concrete sections by programmable calculator," *PCI J.*, **24**(1), 32-54.
Minelli, F. and Plizzari, G.A. (2010), "Shear strength of FRC members with little or no shear reinforcement: a new analytical model", *fib Bulletin*, **57**(1), 211-226.
Narayanan, R. and Darwish, Y. (1987), "Shear in prestressed concrete beams containing steel fibres", *Int. J. Cement Comp. Lightweight Concrete*, **9**(2), 81-90.
Nataraja, M.C., Dhang, N. and Gupta, A.P. (1999), "Stress-strain curves for steel-fiber reinforced concrete under compression", *Cement Concrete Comp.*, **21**(5), 383-390.
Padmarajaiah, S.K. and Ramaswamy, A. (2001), "Behavior of fiber-reinforced prestressed and reinforced high-strength concrete beams subjected to shear", *ACI Struct. J.*, **98**(5), 752-761.
Padmarajaiah, S.K. and Ramaswamy, A. (2004), "Flexural strength predictions of steel fiber reinforced high-strength concrete in fully-partially prestressed beam specimens", *Cement Concrete Comp.*, **26**(4), 275-290.
Rahai, A. and Shokoohfar A. (2012), "Nonlinear shear strength of pre-stressed concrete beams", *Struct. Eng. Mech.*, **41**(4), 441-458.
Spinella, N., Colajanni, P. and La Mendola, L. (2012), "Nonlinear analysis of beams reinforced in shear with stirrups and steel fibers", *ACI Struct. J.*, **109**(1), 53-64.
Susetyo, J. (2009), "Fibre reinforcement for shrinkage crack control in prestressed, precast segmental bridges", Ph.D dissertation, University of Toronto.
Tan, K.H. and Mansur, M.A. (1990), "Shear transfer in reinforced fiber concrete", *J. Mater. Civil Eng.*, **2**(4), 202-214.
Tan, K.H., Murugappan, K. and Paramasivam, P. (1992), "Shear behavior of steel fiber reinforced concrete beams", *ACI Struct. J.*, **89**(6), 3-11.
Tan, K.H., Paramasivam, P. and Murugappan, K. (1996), "Steel fibers as shear reinforcement in patially prestressed beams", *ACI Struct. J.*, **92**(6), 643-651.
Thomas, J. and Ramaswamy, A. (2006), "Shear strength of prestressed concrete T-beams with steel fibers over partial/full depth", *ACI Struct. J.*, **103**(3), 427-435.
Vecchio, F.J. and Collins, M.P. (1986), "Modified compression field theory for reinforced concrete elements subjected to shear", *ACI J. Proc.*, **83**(2), 219-231.
Vecchio, F.J. and Wong, P. (2002), "Vector2 and formworks manual", Publication No. 2002-02, *Dept. Civil Eng. Pub.*, University of Toronto, Toronto, ON, Canada.
Voo, J.Y.L. and Foster, S.J. (2003), "Variable engagement model for fibre reinforced concrete in tension", UNICIV Report No. R-420 June 2003, University of New South Wales, Sydney, Australia.

CC

Notations

A = area of cross section
a/d = ratio of shear span to depth
b_w = web width
d = effective depth of beam
D_f = diameter of steel fiber
d_f = factor of steel fiber shape
E_{cf} = modulus of elasticity of SFRC
E_s = modulus of elasticity of reinforcement and structural steel
f_c' = specified compressive strength of concrete
f_{cr} , $f_{cr,sfrc}$ = stress in concrete and SFRC at cracking
f_{cu}' = cuvic strength of concrete
f_{pc} = compressive strain of concrete at centroid
f_u = tensile strength of reinforcing steel
f_y = yield stress of reinforcing steel
L_f = length of steel fiber
P_{cr} = flexural cracking load
P_{dcr} = diagonal cracking load
P_u = ultimate load
$s_{m\theta}$ = crack spacing
V_f = steel fiber volume ratio
γ_{xy} = average shear strain
δ = deflection
ε_1 = principal tensile strain
ε_2 = principal compressive strain
ε_c' = strain at specified compressive strength of concrete
ε_{cr} = cracking strain
ε_{tu} = ultimate tensile strainof SFRC
ε_y = yield strain of reinforcing steel
θ = angle of inclination of principal axis to longuitudinal direction
ρ_p = ratio of prestressing steel
ρ_s = ratio of ordinary bonded steel

σ_1, σ_1^f = principal tensile stress of concrete and SFRC

Appendix A: Equations

Shear strength equation represented in ACI318-11

$$V_{n,ACI} = \left(0.29\lambda\sqrt{f_c'} + 0.3 f_{pc}\right) b_w d_p + V_p \tag{A1}$$

where, λ is modification factor to reflect the reduced mechanical properties of lightweight concrete, d_p is distance from extreme compression fiber to prestressing steel, and V_p is the vertical component of the effective prestress.

Shear strength equation represented in Model Code 2010

$$V_{n,MC2010} = \left(\frac{0.18k}{\gamma_c}\left[100\rho_l\left(1+7.5\frac{f_{Ftuk}}{f_{ctk}}\right)f_c'\right]^{1/3} + 0.15 f_{pc}\right) b_w d \tag{A2}$$

where, k is a size effect parameter taken as $k = 1+\sqrt{200/d} \le 2.0$, γ_c is the partial safety factor for concrete taken as 1.0 in this study, ρ_l is the reinforcement ratio, f_{Ftuk} is the tensile strength of the concrete assessed at the crack width w=1.5 mm, and f_{ckt} is the tensile strength of concrete taken as $0.33\sqrt{f_c'}$ in this study.

Variable Engagement Model (VEM)

$$f_{tf} = K_f \eta V_f \tau_b \tag{A3}$$

where, f_{tf} is the tensile stress of SFRC, K_f is a global orientation factor that is a function of the current crack opening displacement, η is the aspect ratio of fibers, that is, $\eta = L/D$, V_f is the volumetric fraction of fibers, and τ_b is the bond stress between fibers and concrete matrix that can be taken as $0.8\sqrt{f_c'}$ for hooked fibers. Also, K_f can be calculated as follows.

$$K_f = \frac{1}{\pi}\tan^{-1}\left[w/\left(\alpha_I L\right)\right]\left(1-\frac{2w}{L}\right)^2 \tag{A4}$$

where, w is the crack opening displacement, and α_I is a fiber engagement coefficient that can be taken as α_I=1/(3.5η). The fiber length (L) shall not be larger than $L_{crit} = \frac{D}{2}\frac{\sigma_{fu}}{\tau_b}$, because it is assumed that all fibers are pulled out from the concrete in the formulation of Eq. (A4), where σ_{fu} is the tensile strength of a fiber.

Appendix B

Table A1 SFRPSC specimens and test results reported in Narayanan and Darwish

Specimen name	b_w (mm)	d (mm)	a/d	f_{cu} (MPa)	ρ_s	ρ_p	P_e (kN)	f_{pc} (MPa)	V_f (%)	l_f (mm)	d_f (mm)	F	Fiber shape	Shear strength (MPa)
P1	85.0	114.0	3.0	44.7	0.0233	0.0079	64	5.02	0.0	30.0	0.30	0.00	crimped	2.79
P2	85.0	114.0	3.0	55.0	0.0233	0.0079	64	5.02	0.3	30.0	0.30	0.23	crimped	3.72
P3	85.0	114.0	3.0	56.0	0.0233	0.0079	64	5.02	0.6	30.0	0.30	0.45	crimped	4.13
P4	85.0	114.0	3.0	54.4	0.0233	0.0079	64	5.02	0.9	30.0	0.30	0.68	crimped	5.16
P5	85.0	109.0	3.0	56.8	0.0244	0.0083	64	5.02	1.2	30.0	0.30	0.90	crimped	6.05
P6	85.0	109.0	3.0	55.3	0.0244	0.0083	64	5.02	1.5	30.0	0.30	1.13	crimped	5.72
P7	85.0	114.0	3.0	66.2	0.0233	0.0079	64	5.02	2.0	30.0	0.30	1.50	crimped	5.27
P9	85.0	114.0	3.0	65.0	0.0233	0.0079	48	3.76	0.3	30.0	0.30	0.23	crimped	3.62
P10	85.0	114.0	3.0	67.8	0.0233	0.0079	48	3.76	0.6	30.0	0.30	0.45	crimped	4.13
P11	85.0	114.0	3.0	59.1	0.0233	0.0079	48	3.76	0.9	30.0	0.30	0.68	crimped	5.72
P12	85.0	114.0	3.0	61.3	0.0233	0.0079	48	3.76	1.2	30.0	0.30	0.90	crimped	5.17
P13	85.0	114.0	3.0	66.2	0.0233	0.0079	48	3.76	2.0	30.0	0.30	1.50	crimped	5.11
P15	85.0	114.0	3.0	63.3	0.0233	0.0079	32	2.51	0.3	30.0	0.30	0.23	crimped	3.10
P16	85.0	114.0	3.0	66.3	0.0233	0.0079	32	2.51	0.6	30.0	0.30	0.45	crimped	4.37
P17	85.0	114.0	3.0	53.8	0.0233	0.0079	32	2.51	0.9	30.0	0.30	0.68	crimped	4.78
P18	85.0	114.0	3.0	54.8	0.0233	0.0079	32	2.51	1.2	30.0	0.30	0.90	crimped	5.14
P19	85.0	114.0	3.0	61.5	0.0233	0.0079	32	2.51	2.0	30.0	0.30	1.50	crimped	5.37
P20	85.0	114.0	3.0	63.5	0.0233	0.0079	32	2.51	2.5	30.0	0.30	1.88	crimped	5.62
P21	85.0	100.0	3.0	63.3	0.0266	0.0181	80	6.27	0.3	30.0	0.30	0.23	crimped	5.46
P22	85.0	100.0	3.0	66.3	0.0266	0.0181	80	6.27	0.6	30.0	0.30	0.45	crimped	6.29
P23	85.0	100.0	3.0	53.8	0.0266	0.0181	80	6.27	0.9	30.0	0.30	0.68	crimped	5.92
P24	85.0	100.0	3.0	54.8	0.0266	0.0181	80	6.27	1.2	30.0	0.30	0.90	crimped	6.04
P25	85.0	100.0	3.0	60.0	0.0266	0.0181	80	6.27	2.0	30.0	0.30	1.50	crimped	7.16
P26	85.0	100.0	3.0	66.0	0.0266	0.0181	80	6.27	2.5	30.0	0.30	1.88	crimped	6.75